THE JOURNAL OF BIOLOGICAL CHEMISTRY VOL. 289, NO. 45, pp. 31121–31135, November 7, 2014

Identification of *14-3-3β* Gene as a Novel miR-152 Target Using a Proteome-based Approach*

Received for publication, February 24, 2014, and in revised form, August 28, 2014 Published, JBC Papers in Press, September 16, 2014, DOI 10.1074/jbc.M114.556290

Simon Jasinski-Bergner[‡1], Franziska Stehle[‡1], Evamaria Gonschorek[‡], Jana Kalich[‡], Kristin Schulz[‡], Stefan Huettelmaier[§], Juliane Braun[§], and Barbara Seliger[‡2]

From the [‡]Institute of Medical Immunology, Martin Luther University Halle-Wittenberg, 06112 Halle and the [§]Institute of Molecular Medicine, Martin Luther University Halle-Wittenberg, 06120 Halle, Germany

Background: miR-152 regulates *HLA-G* and *HLA-C*, which act inhibitory to NK and T cells, thereby altering the immunogenicity of tumors.
Results: Applying a proteome-based approach, novel miR-152 targets were identified, *e.g.* anti-apoptotic *14-3-3β* overexpressed in certain tumors.
Conclusion: The known tumor-suppressive miR-152 regulates *14-3-3β*, thereby enhancing the sensitivity of tumor cells for apoptosis.
Significance: miR-152 exerts a dual role by altering the immunogenicity and the tumorigenicity.

Recent studies demonstrated that miR-152 overexpression down-regulates the nonclassical human leukocyte antigen (HLA) class I molecule *HLA-G* in human tumors thereby contributing to their immune surveillance. Using two-dimensional gel electrophoresis followed by MALDI-TOF mass spectrometry, the protein expression profile of HLA-G$^+$, miR-152^{low} cells, and their miR-152-overexpressing (miR^{high}) counterparts was compared leading to the identification of 24 differentially expressed proteins. These were categorized according to their function and localization demonstrating for most of them an important role in the initiation and progression of tumors. The novel miR-152 target 14-3-3 protein β/α/YWHAB (14-3-3β) is down-regulated upon miR-152 overexpression, although its overexpression was often found in tumors of distinct origin. The miR-152-mediated reduction of the *14-3-3β* expression was accompanied by an up-regulation of BAX protein expression resulting in a pro-apoptotic phenotype. In contrast, the reconstitution of *14-3-3β* expression in miR-152^{high} cells increased the expression of the anti-apoptotic *BCL2* gene, enhances the proliferative activity in the presence of the cytostatic drug paclitaxel, and causes resistance to apoptosis induced by this drug. By correlating clinical microarray data with the patients' outcome, a link between *14-3-3β* and *HLA-G* expression was found, which could be associated with poor prognosis and overall survival of patients with tumors. Because miR-152 controls both the expression of *14-3-3β* and *HLA-G*, it exerts a dual role in tumor cells by both altering the immunogenicity and the tumorigenicity.

* This work was supported by Deutsche Forschungsgemeinschaft Grant GRK 1591, the Mildred Scheel Cancer Research Foundation, the Else Kroener Fresenius Foundation, and the intramural Roux program of the Martin Luther University Halle-Wittenberg.
[1] Both authors contributed equally to this work.
[2] To whom correspondence should be addressed: Martin-Luther-University-Halle-Wittenberg, Institute of Medical Immunology, Magdeburger Str. 2, 06112 Halle/Saale, Germany. Tel.: 49-345-557-4054; Fax: 49-345-557-4055; E-mail: barbara.seliger@uk-halle.de.

MicroRNAs (miRs)[3] are small 22-nucleotide-long noncoding RNAs representing key regulators of the post-transcriptional gene regulation (1). So far, more than 2500 human miRs are listed at the mirbase on-line database (2). The sequence-specific binding to a target mRNA is determined by the "seed" region of the miRs (3) and predominantly occurs at the 3′-untranslated region (UTR) of the target mRNA.

Recently, members of the miR-148 family, miR-148A, miR-148B, and miR-152, have been demonstrated to regulate the immune modulatory nonclassical human leukocyte antigen (HLA) class I molecule, *HLA-G* (4). Under physiologic conditions, *HLA-G* is selectively expressed on fetal tissues, thereby regulating the feto-maternal immune tolerance, and in adults on immune-privileged organs. During the last few years, a role of *HLA-G* as immune modulatory molecule in several diseases such as autoimmune disorders, viral infections, and tumors has been described. *HLA-G* expression was often detected on solid and hematopoietic tumors, which could be associated with disease progression and poor patient survival (5–7). In addition to the regulation of *HLA-G*, the *HLA-C* antigen is also regulated by members of the miR-148 family (8). Because *HLA-G* and *HLA-C* are both ligands for inhibitory NK cell receptors (9, 10), the miR-148 family is an important regulator of an effective immune response against tumor cells and also against viral infections. The expression of miR-148 family members, including miR-152, is often down-regulated in tumors of distinct origin, including prostate, ovarian, endometrial, and colorectal cancers. This was associated with advanced tumor staging and grading as well as reduced overall survival of tumor patients. In contrast, high miR-152 expression levels were associated with increased apoptosis, decreased cell proliferation, invasion, and angiogenesis (11–14). Furthermore, plasma levels of miR-152 in tumor patients could be used as predictors of patient outcome (15). This is in line with the association of decreased miR-

[3] The abbreviations used are: miR, microRNA; CFSE, carboxyfluorescein succinimidyl ester; luc, luciferase; RCC, renal cell carcinoma; 2DE, two-dimensional gel electrophoresis; qPCR, quantitative PCR; ACN, acetonitrile.

152 expression and chemotherapy resistance. Thus, miR-152 represents the tumor suppressor miR, which is often silenced by DNA hypermethylation in tumors (12). The following question is addressed. Which genes relevant for tumor cell fate and tumor progression are directly regulated by miR-152? miR-152 was overexpressed in the miR-152^{low} HLA-G^{+} choriocarcinoma cell line JEG-3 (4, 16). Because miRs impair protein synthesis from targeted mRNAs, 2DE-based proteomic approaches in combination with mass spectrometry were employed to identify novel miR-152 targets by comparative analyses of the protein expression patterns of miR-152$^{low/high}$ tumor cells. One of these targets, *14-3-3β* (14-3-3 protein β/α/YWHAB), was validated and functionally characterized. miR-152-mediated inhibition of *14-3-3β* expression was accompanied by reduced growth capacity and enhanced apoptosis sensitivity in the presence of the chemotherapeutic drug paclitaxel, which could be reverted by restoration of *14-3-3β* expression via down-regulation of the pro-apoptotic protein BAX and the up-regulation of the expression of the anti-apoptotic gene *BCL2*. In addition, *14-3-3β* and *HLA-G* expression in selected tumor entities was linked to a reduced survival of patients.

MATERIALS AND METHODS

Cell Lines and Tissue Culture—The HLA-G negative human embryonal kidney cell line HEK293T and the HLA-G positive choriocarcinoma cell line JEG-3 were purchased from the American Type Culture Collection (ATCC® CRL-3216™ and ATCC® HTB-36™, Manassas, VA). The cell lines MZ1257RC, MZ1795RC, and MZ1851RC as well as buf1088, FM82, and WM1862 were established from patients with renal cell carcinoma (RCC) or metastatic melanoma, respectively, and have been described recently (17–20). With the exception of JEG-3 cells, which were maintained in RPMI 1640 medium (Invitrogen), all other cell lines were cultured in DMEM (Invitrogen) supplemented with 10% (v/v) fetal bovine serum (FCS) (PAA; Pasching, Austria), 2 mM L-glutamine (Lonza, Basel, Switzerland), and 1% (v/v) penicillin/streptomycin (PAA).

Isolation of DNA, RNA, and miR—DNA and total cellular RNA were isolated using the QIAamp DNA mini kit (Qiagen, Hilden, Germany) and the TRIzol reagent (Invitrogen) according to the manufacturers' protocols, respectively. RNA was treated with DNase I (New England Biolabs) for 30 min at room temperature, inactivated with EDTA (5 mM final concentration), and then incubated at 75 °C for 10 min.

2DE, Protein Visualization, and Image Analysis—Frozen cell pellets (1×10^7 cells/sample; three biologic replicates) were harvested, washed three times in PBS (PAA), and stored at −80 °C. Proteins were extracted with lysis buffer in 7 M urea (AppliChem, Darmstadt, Germany), 2 M thiourea (Sigma), 0.2 M dimethylbenzylammonium propane sulfonate (NDSB 201, Merck), 1% dithiothreitol (DTT; AppliChem, Darmstadt, Germany), 4% CHAPS (AppliChem), 0.5% Pharmalyte (Amersham Biosciences), and a trace of bromphenol blue (Serva Electrophoresis, Heidelberg, Germany). The lysate was sonicated using two cycles of five impulses (0.5 s/impulse) at 100% power (Bandelin UW 2070 sonicator, MS 73 needle; Bandelin, Berlin, Germany) and then cleared by centrifugation (18,000 × *g*, 90 min, 15 °C). Total protein concentration was determined as described previously (19). Samples (500 μg of protein in a volume of 350 μl of lysis buffer) were applied to IPG strips (pH 3–10 NL, 18 cm, GE Healthcare) by in-gel rehydration and covered with 450 μl of Immobiline DryStrip Cover Fluid (GE Healthcare). After 2 h of rehydration, isoelectric focusing was carried out at 20 °C on an Ettan IPGphor 2 unit (GE Healthcare) at the following settings: 30 V for 10 h, 500 V for 1 h, 1000 V for 1 h, 5000 V for 1 h, and 8000 V up to a total of 45,000 V*h. The IPG strips were subjected to the strip equilibration procedure, which was performed by incubating the strips for 15 min in 12 ml of equilibration buffer (6 M urea, 2% SDS, 50 mM Tris-HCl (pH 8.8), 30% glycerol) supplemented with 1.5% DTT followed by 15 min in 12 ml of equilibration buffer supplemented with 4.8% iodoacetamide (all chemicals by AppliChem). SDS-PAGE separation was performed using a PROTEAN plus Dodeca Cell (Bio-Rad) with gels of 1.5 mm thickness and an acrylamide concentration of 13%. Strips were fixed on vertical SDS-polyacrylamide gels with 1.5% low melting agarose (BioLine GmbH, Luckenwalde, Germany) and traces of bromphenol blue. Electrophoresis was performed with constant voltage (20 V for 1 h; 120 V for 15 h) at 10 °C.

The gels were then stained with colloidal Coomassie Blue staining solution (10% ammonium sulfate, 0.12% Coomassie Brilliant Blue G-250 (AppliChem), 10% phosphoric acid, 20% methanol (Merck KGaA) (28)), and thereafter destained by washing in double distilled H_2O. All gels were scanned (UMAX Image Scanner, GE Healthcare) at a resolution of 600 dpi and stored as TIFF-images.

Two-dimensional gel image analysis was performed using Delta2D software version 4.0.8 (DECODON GmbH, Greifswald, Germany). All gel images were matched with the Delta2D software, and a synthetic fusion gel was prepared. Final spot detection was performed on the fused gel. The resulting spot pattern was assigned to each of the gels in the experiment. Student's *t* test was performed to assess the statistical significance of differentially expressed proteins. Based on average spot volume ratio, spots whose relative expression is changed at least 2-fold (increase or decrease) at 95% confidence level (*t* test; $p < 0.05$) were considered to be significant and subsequently subjected to further analysis.

In-gel Digestion and MS—Digestion with trypsin and subsequent spotting of peptide solutions onto the MALDI targets were performed as described previously (19) with slight modifications. For protein identification, the proteins were excised from stained two-dimensional gels using the Herolab spot hunter (Herolab GmbH, Wiesloch, Germany) and destained by addition of 50% (v/v) ACN. Gel pieces were washed twice with 100 μl of 50% (v/v) ACN and once with 100 μl of 100% ACN. After drying, 5 μl of trypsin solution containing 17 ng/μl trypsin (Promega, Madison, WI) in 25 mM NH_4CO_3 supplemented with 0.4 mM $CaCl_2$ was added and incubated on ice for 2 h followed by an incubation overnight at 37 °C. If necessary, 5 μl of 25 mM NH_4CO_3 supplemented with 0.4 mM $CaCl_2$ was added to keep gel pieces hydrated throughout the digest. Gel pieces were agitated by sonicating in a water bath for 10 min before 1 μl of the supernatant (containing tryptic peptides) was mixed with 1 μl of α-cyano-4-hydroxycinnamic acid matrix (saturated at room temperature in 50% ACN, 0.1% TFA), and 1 μl of this solution was directly spotted on the MALDI target and allowed to dry.

TABLE 1
Differentially expressed proteins upon miR-152 overexpression in JEG-3 cells determined by 2DE-based proteomic profiling and mass spectrometry

Spot no.	Protein name	Official gene symbol	Protein accession no.	Sequence coverage	Mascot score	x-Fold change	Cellular function	Cellular compartment
				%				
02	Thioredoxin	*TXN*	P10599	80	106	2.2	Electron transport; transcription regulation	Cytoplasm, nucleus, secreted
04	Nucleoside diphosphate kinase A	*NME1*	P15531	69	94	2.3	differentiation, endocytosis, neurogenesis, nucleotide metabolism	Cytoplasm, nucleus
05	Elongation factor 2	*EEF2*	P13639	31	151	13.2	Protein biosynthesis	Cytoplasm
06	Ezrin	*EZR*	P15311	34	172	2.3	Cell shape	Cell membrane, cell projection, cytoplasm, cytoskeleton, membrane
07	Endoplasmin	*HSP90B1*	P14625	22	132	0.5	Chaperone	Endoplasmic reticulum
08	Fascin	*FSCN1*	Q16658	48	176	2.0	Actin-binding, cell migration, cell proliferation	Cell junction, cell projection, cytoplasm, cytoskeleton
10	Keratin, type II cytoskeletal 8	*KRT8*	P05787	48	195	0.5	Cytoskeleton organization	Cytoplasm, intermediate filament, keratin, nucleus
11	60-kDa heat shock protein, mitochondrial	*HSPD1*	P10809	34	140	0.4	Mitochondrial protein import and macro-molecular assembly	Mitochondrion
13	Heat shock protein HSP 90-α	*HSP90AA1*	P07900	18	96	0.3	stress response	Cytoplasm
14	Multifunctional protein ADE2	*PAICS*	P22234	28	93	2.5	Purine biosynthesis	Cytosol
16	α-Enolase	*ENO1*	P06733	41	115	0.4	Glycolysis, plasminogen activation, transcription regulation	Cell membrane, cytoplasm, membrane, nucleus
17	Eukaryotic translation initiation factor 2 subunit 1	*EIF2S1*	P05198	35	105	0.3	Protein biosynthesis, translation regulation	Cytosol, nucleus
18	Annexin A2	*ANXA2*	P07355	36	102	2,7	Calcium-regulated membrane-binding protein, angiogenesis, heat-stress response	Basement membrane, extracellular matrix, secreted
19	Protein-disulfide isomerase A6	*PDIA6*	Q15084	49	180	0.2	Chaperone, isomerase	Cell membrane, endoplasmic reticulum
20	26 S proteasome non-ATPase regulatory subunit 14	*PSMD14*	O00487	46	106	2.4	DNA damage, DNA repair, Ubl conjugation pathway	Proteasome
21	Calreticulin	*CALR*	P27797	24	65	2.8	Chaperone	Cytoplasm, endoplasmic reticulum, extracellular matrix, sarcoplasmic reticulum, secreted
22	Proliferating cell nuclear antigen	*PCNA*	P12004	68	145	0.4	DNA damage, DNA repair, DNA replication	Nucleus
24	Elongation factor Tu, mitochondrial	*TUFM*	P49411	44	165	0.4	Protein biosynthesis	Mitochondrion
25	Protein-disulfideisomerase A3	*PDIA3*	P30101	25	107	0.4	Isomerase	Endoplasmic reticulum
26	14-3-3 protein ϵ	*YWHAE*	P62258	47	102	0.5	Adapter protein, regulation of signaling pathways	Cytoplasm
27	14-3-3 protein β/α	*YWHAB*	P31946	31	74	0.5	Adapter protein, regulation of signaling pathways	Cytoplasm
29	Growth factor receptor-bound protein 2	*GRB2*	P62993	36	63	0.4	Adapter protein, link between cell surface growth factor receptors and the Ras signaling pathway	Cytoplasm, endosome, Golgi apparatus, nucleus
30	ES1 protein homolog, mitochondrial	*C21orf33*	P30042	45	90	2.4		Mitochondrion
31	Keratin, type I cytoskeletal 19	*KRT19*	P08727	38	152	0.5	Organization of myofibers	Intermediate filament, keratin

Spectra were calibrated externally using Bruker's peptide calibration standard II (Bruker Daltonics Inc., Bremen, Germany). MALDI-TOF-MS was performed on an ultrafleXtreme™ mass spectrometer (Bruker Daltonics Inc.) in positive reflector mode using an accelerating voltage of 25 kV. Spectra processing was performed with FlexAnalysis (3.3.80.0) software for resolution-based peak detection using default settings.

The PMF dataset were analyzed using the MASCOT search engine with the following parameters: (i) *Homo sapiens* sequences; (ii) fixed modification, carbamidomethylation of cysteines; (iii) cleavage enzyme, trypsin; (vi) a maximum of one missed cleavage was allowed; and mass tolerance (monoisotopic) was ± 50.0 ppm. Target identification was based on the overall sequence coverage of matching peptide fragments. Proteins were assigned when the MASCOT score exceeded 57 according to the MASCOT-defined significance threshold for false-positive events at $p < 0.05$.

The heterogeneous set of the identified significant differentially expressed proteins was analyzed using gene ontology (GO miner software (29)), which provides information about gene function and cellular localization. The results are listed in Table 1 .

Semi-quantitative and Quantitative PCR—cDNA was synthesized from 2 μg of total cellular RNA using random hexamer primers (Fermentas, Mannheim, Germany) and the RevertAid™ H Minus First Strand cDNA synthesis kit according to the manufacturer's instructions (Fermentas, St. Ingbert, Germany). For miR-specific cDNA synthesis, miR-specific stem-loop primers altered after Chen *et al.* 2005 (21) were employed (22). PCR was performed with target-specific primers using Platinum® SYBR® Green qPCR SuperMix-UDG (Invitrogen). The reverse transcription and PCRs were carried out in a 96-well labcycler (Sensoquest, Goettingen, Germany); the qPCRs for the quantification of miRs were performed in a Bio-Rad 96-well iCycler (Bio-Rad), and the relative quantification of mRNAs was determined in a rotor gene cycler (Qiagen). All reactions were run as triplicates of biologic replicates. For qPCR of miRs, the absolute copy numbers were determined against the respective external miR-specific TOPO-TA plasmid standards (Invitrogen), which were generated by cloning the stem-loop PCR product of the miR of interest into this plasmid. Relative mRNA expression levels for specific genes were normalized to GAPDH. All oligonu-

TABLE 2
Oligonucleotides applied in this study
fw is forward, and rev is reverse.

Primer	Application	Sequence (5′ → 3′)	Condition
miR-141	Stem-loop primer	GTCGTATCCAGTGCAGGGTCCGAGGTATTCGCACTGGATACGACCCATCT	42 °C
miR-141 fw	qPCR	GCCCTAACACTGTCTGGTAA	60 °C
miR-152	Stem-loop primer	GTCGTATCCAGTGCAGGGTCCGAGGTATTCGCACTGGATACGACCCAAGT	42 °C
miR-152 fw	qPCR	GCCCTCAGTGCATGACAGA	60 °C
miR-541	Stem-loop primer	GTCGTATCCAGTGCAGGGTCCGAGGTATTCGCACTGGATACGACAGTCCA	42 °C
miR-541 fw	qPCR	GCCCTGGTGGGCACAGAATC	60 °C
Stem loop PCR rev primer	qPCR	GTGCAGGGTCCGAGGT	60 °C
Clone miR-152fw	Cloning	AAACTCGAGTTCTGGGTCCGTTTGGAGT	60 °C
Clone miR-152 rev	Cloning	AAAGAATTCGTTCTGCCCAGCCCT	60 °C
Clone miR-541 fw	Cloning	AAACTCGAGAGAATTTCCAGAAGCAACAG	60 °C
Clone miR-541 rev	Cloning	AAAGAATTCCCAGGATCCCTCAAAGAGTA	60 °C
Clone *YWHAB* CDS fw	Cloning	AAAGGATCCTTCGCTCGGAAGGGTCTTTG	58 °C
Clone *YWHAB* CDS rev	Cloning	AAAACGCGTTTTCCTAGGCTGAGGCTGTG	58 °C
qPCR*HLAG* fw (53)	qPCR	TTGCTGGCCTGGTTGTCCTT	60 °C
qPCR*HLAG* rev (53)	qPCR	TTGCCACTCAGTCCCACACAG	60 °C
Forward *GAPDH* (Fermentas)	qPCR	CAAGGTCATCCATGACAACTTTG	60 °C
Reverse *GAPDH* (Fermentas)	qPCR	GTCCACCACCCTGTTGCTGTAG	60 °C
qPCR *YWHAB* fw	qPCR	GGAAGGAAGAGGTCATCTCGC	60 °C
qPCR *YWHAB* rev	qPCR	TGCTTCTCTATCCACAGCCG	60 °C
*HLA-G*miTrap fw	Cloning	AAAGAATTCAAACAGCTGCCCTGTGT	60 °C
*HLA-G*miTRAP rev	Cloning	AAACTCGAGCTCTCAAATTTCAGGAATC	60 °C
miTRAP *YWHAB* fw	Cloning	AAAGAATTCTTACTGAGCACCTTGGTGAG	58 °C
miTRAP *YWHAB* rev	Cloning	AAACTCGAGTTCACAACCACGGGTGTGCT	58 °C
luc *YWHAB* fw	Cloning	AAAACTAGTTTACTGAGCACCTTGGTGAG	58 °C
luc *YWHAB* rev	Cloning	AAAACGCGTTTCACAACCACGGGTGTGCT	58 °C
Δ152#1 fw	Fusion PCR	AATGCAGTAGTGAATGTGGAAGCTCTTTTCTTGCTTTGTT	
Δ152#1 rev	Fusion PCR	AACAAAGCAAGAAAAGAGCTTCCACATTCACTACTGCATT	
qPCR CDK1 fw	qPCR	AGCCGGGATCTACCATACCC	60 °C
qPCR *CDK1* rev	qPCR	CTGGCAAGGCCAAAATCAGC	60 °C
qPCR *CDK2* fw	qPCR	CACTGAGACTGAGGGTGTGC	60 °C
qPCR *CDK2* rev	qPCR	GGAGGATTTCAGGAGCTCGG	60 °C
qPCR *CDK4* fw	qPCR	GGCTTTACTGAGGCGACTGG	60 °C
qPCR *CDK4* rev	qPCR	TGGTCGGCTTCAGAGTTTCC	60 °C
qPCR *CDK6* fw	qPCR	TCACACCGAGTAGTGCATCG	60 °C
qPCR *CDK6* rev	qPCR	GACTTCGGGTGCTCTGTACC	60 °C
qPCR *CCNB* fw	qPCR	AAGGCGAAGATCAACATGGC	60 °C
qPCR *CCNB* rev	qPCR	CACAGGTCTTCTTCTGCAGGG	60 °C
qPCR *CCNA* fw	qPCR	TGTCACCGTTCCTCCTTGG	60 °C
qPCR *CCNA* rev	qPCR	ACTGACATGGAAGACAGGAACC	60 °C
qPCR *CCND1* fw	qPCR	CAGAAGCGAGAGCCGAGC	60 °C
qPCR *CCND1* rev	qPCR	CCACGAACATGCAAGTGGC	60 °C
qPCR *CCNE* fw	qPCR	CCATCATGCCGAGGGAGC	60 °C
qPCR *CCNE* rev	qPCR	TTTGCCCAGCTCAGTACAGG	60 °C
qPCR *BAX* fw	qPCR	CTGAGCAGATCATGAAGACAGG	60 °C
qPCR *BAX* rev	qPCR	CTCCATGTTACTGTCCAGTTCG	60 °C
qPCR *BAD* fw	qPCR	TGAGCCGAGTGAGCAGGAAG	60 °C
qPCR *BAD* rev	qPCR	ATGATGCTTGCCGGAGCCTG	60 °C
qPCR *BCL2* fw	qPCR	GGAGGATTGTGGCCTTCT	60 °C
qPCR *BCL2* rev	qPCR	TGCCGGTTCAGGTACTCA	60 °C
qPCR *Survivin* fw	qPCR	CACCGCATCTCTACATTCAAGA	60 °C
qPCR *Survivin* rev	qPCR	CAAGTCTGGCTCGTTCTCAGT	60 °C
qPCR *Mcl1* fw	qPCR	GAGTTGTACCGGCAGTCGCT	60 °C
qPCR *Mcl1* rev	qPCR	AGTTTGTTACGCCGTCGCTG	60 °C
qPCR *PTEN* fw	qPCR	TCCACAAACAGAACAAGATGCT	60 °C
qPCR *PTEN* rev	qPCR	CTCTGGATCAGAGTCAGTGGTG	60 °C
qPCR *TP53* fw	qPCR	CCTGTGCAGCTGTGGGTTGATTCC	65 °C
qPCR *TP53* rev	qPCR	GGATGGTGGTACAGTCAGAGCCAA	65 °C
152decoyse1	Hybridization/cloning	GATCCGGACGGCGCTAGGATCATCAACCCAAGTTCTGTCATGACTGACAAGTATT	
152decoyse2	Hybridization/cloning	CTGGTCACAGAATACAACCCAAGTTCTGTCATGACTGACAAGATGATCCTAGCGCCGTCTTTTTTG	
152decoyas2	Hybridization/cloning	GAATTCAAAAAAGACGGCGCTAGGATCATCTTGTCAGTCATGACAGAACTTGGGTTGTATTCTGTG	
152decoyas1	Hybridization/cloning	ACCAGAATACTTGTCAGTCATGACAGAACTTGGGTTGATGATCCTAGCGCCGTCCG	

cleotides used for the mRNA and miR expression profiling are listed in Table 2.

For analysis of the gene expression involved in regulation of cell cycle and apoptosis, cells were synchronized by serum starvation (0.5% FCS (v/v)) for 48 h, and the cells were then cultured for 48 h in complete medium (10% FCS) before harvesting for RNA extraction.

Protein Extraction and Western Blot Analysis—Protein extraction and Western blot analyses were performed as described elsewhere (23). 50 or 70 μg of protein/lane were separated on 12% or 14% SDS-polyacrylamide gels and subsequently transferred onto nitrocellulose membranes (Schleicher & Schuell). Membranes were processed as described previously (23) using target protein-specific primary antibodies directed against 14-3-3β (polyclonal antibody C-20; Santa Cruz Biotechnology) and the monoclonal antibodies (mAb) directed against HLA-G (MEM-G/1; EXBIO, Prague, Czech Republic), BAX, and cleaved caspase 3 (Cell Signaling) in combination with horseradish peroxidase (HRP)-conjugated secondary antibodies (DAKO, Hamburg, Germany). Staining with an anti-GAPDH antibody (Cell Signaling) served as loading control, and the relative protein expression level for each target was defined using

AIDA software (Raytest, Sprockhoevel, Germany). Protein bands were visualized with the Lumi-Light Western blotting substrate (Roche Applied Science) and recorded with an LAS 3000 CCD camera system (FUJIFILM, Düsseldorf, Germany).

Flow Cytometry—Flow cytometry was performed for analysis of cell proliferation and apoptosis induction using 5,6-carboxyfluorescein diacetate-succinimidyl ester (CFSE) staining (Invitrogen) and allo-phycocyanine-conjugated annexin V (Pharmingen) in combination with 7-amino-actinomycin D staining (Pharmingen), respectively, according to the manufacturer's instructions as recently described (24). To evaluate cell proliferation, 3×10^6 cells were labeled with CFSE for 15 min at 37 °C in 10 ml of phosphate-buffered saline (PBS) supplemented with 0.3% FCS, according to the manufacturer's instructions, and finally seeded in 6-well microtiter plates (Techno Plastic Products AG, TPP, Trasadingen, Switzerland). After 24 h, the mean specific fluorescence intensity of the CFSE-labeled cells was analyzed before the cells were treated with 25 nM paclitaxel (Taxol®, Bristol-Myers Squibb, New York) or DMSO in a time kinetic fashion in the absence of any antibiotics. After 24, 48, and 72 h of treatment, cells were analyzed by flow cytometry.

Cell cycle analysis was performed with synchronized cells as described above. Nuclei were isolated by incubation of cells in 10 mM citric acid supplemented with 0.5% (w/v) Tween 20 for 20 min at 4 °C. After washing, the nuclei were fixed by adding ice-cold ethanol for 24 h at 4 °C. Nuclei were treated with 300 μl of RNase A (1 mg/ml, Sigma) for 10 min at room temperature prior to staining with propidium iodide (5 μl, 2 mg/ml). Cells were analyzed using the LSRfortessa flow cytometer and the FACSDiva software (both from BD Biosciences).

For determination of apoptosis induction, 1×10^5 JEG-3 cells/well were cultured in 6-well microtiter plates (Techno Plastic Products AG, TPP) for 72 h without antibiotics followed by flow cytometry after staining of cells with allo-phycocyanine-annexin V (Pharmingen) and 7-amino-actinomycin D (Pharmingen) according to the manufacturer's instructions (Pharmingen). Stained cells were analyzed on an LSRfortessa flow cytometer (BD Biosciences) in combination with the FACSDiva software package (BD Biosciences) and the Kaluza® flow analysis software (Beckman-Coulter, Krefeld, Germany). The data were either expressed as mean specific fluorescence intensities, histograms, or as percentage of positive cells.

Viability Assay—To determine the viability of the transfectants upon treatment with paclitaxel, an 2,3-bis-(2-methoxy-4-nitro-5-sulfophenyl)-2*H*-tetrazolium-5-carboxanilide (XTT) assay was performed according to the manufacturer's instructions (cell proliferation kit II, Roche Applied Science) using 3000 cells/well in 150 μl of media. Cell viability was analyzed after incubation of cells for 72 h in the absence and presence of paclitaxel (0–20 μM) using a microplate reader (MRX-TC, DYNEX Technologies, Denkendorf, Germany). The absorbance values were expressed as a percentage of the DMSO-treated control group, and IC_{50} values were calculated as published by Stehle *et al.* (24).

Generation of 14-3-3β and miR Expression Vectors and Cell Transfection—For generation of the *14-3-3β* expression vector, cDNA from JEG-3 cells was utilized as template for PCR (primer sequences listed at Table 2). The resulting PCR product was cloned into the pMIR-REPORT vector (Ambion, Austin, TX) by restriction with BamHI and MluI (Fermentas) replacing the luciferase (luc) gene. The miR genes and their flanking regions were cloned into the pmR-m-cherry vector (Clontech) using the restriction enzymes XhoI and EcoRI (Fermentas). JEG-3 cells were stably transfected with the miR, the *14-3-3β* expression vector, and the respective mock vector controls, using the Effectene transfection reagent (Qiagen; Hilden, Germany) according to the manufacturer's protocol.

Luciferase Reporter Gene Assay and Cell Transfection—For the luc reporter gene assays, the 3′-UTR of *14-3-3β* was inserted downstream of the luc reporter gene into the pMiR Report vector (Invitrogen) using the restriction enzymes SpeI and MluI (New England Biolabs). To determine the specificity of miR and target interaction, the respective miR-binding site was deleted within the luc reporter gene construct by fusion PCR. To block miR-152, a respective decoy vector was generated according to Haraguchi *et al.* (25) by hybridization and cloning of complementary oligonucleotides (Table 2) into the pLVX-IRES-ZsGreen (Clontech).

For transfection, 1×10^4 HEK293T cells were seeded into flat bottom 96-well plates, incubated for 24 h at 37 °C, and then transfected with either the miR expression vector or the mock control using the Effectene transfection reagent (Qiagen). After 24 h of incubation at 37 °C, a second transfection was performed using the luc reporter gene constructs and the β-galactosidase (β-gal) vector, the latter serving as control for normalization of transfection efficacy. 72 h after seeding, the cells were harvested with lysis buffer (Promega, Madison, WI). The luc and β-gal activities were determined with a luminometer (Microlumat Plus CB 96V, Berthold Technologies, Bad Wildbad, Germany) using commercially available enzyme assays (Promega) as described recently (23). The results were expressed as a quotient of the luc and β-gal activities.

miR Enrichment Assay (miTRAP)—The miTRAP technology has recently been established and described in detail (26). Briefly, the 3′-UTRs of *14-3-3β* and *HLA-G* were cloned upstream of a sequence encoding for four MS2 loops using the restriction enzymes XhoI and EcoRI (Fermentas), *in vitro* transcribed with riboprobe (Promega), purified with the MEGAclear™ kit (Ambion), and then used for the enrichment of specific miRs from MZ2905RC cell lysate (HLA-G $mRNA^+$/$protein^-$ (7)). First, 500 pmol of fusion protein consisting of MS2 loop and maltose-binding protein domains was coupled to amylose beads (Amylose Resin; New England Biolabs) and purified as described elsewhere (27). After washing, a blocking step with bovine serum albumin (New England Biolabs) and yeast tRNA (Promega) was performed. Then after washing, 20 pmol of *in vitro* transcribed RNA were employed as bait/pulldown and loaded onto the beads. After washing, the beads were incubated with 500 μl of cell lysate (equal to lysate of $3.5 \cdot 10^6$ cells) followed by extensive washing and RNA extraction. The miR enrichment was validated by respective qPCR. RNA extraction and cDNA synthesis were performed as described by Braun *et al.* (26). The principle of this novel experiment is shown in Fig. 8*A*. The usage of terminal MS2 loops ensures the formation of

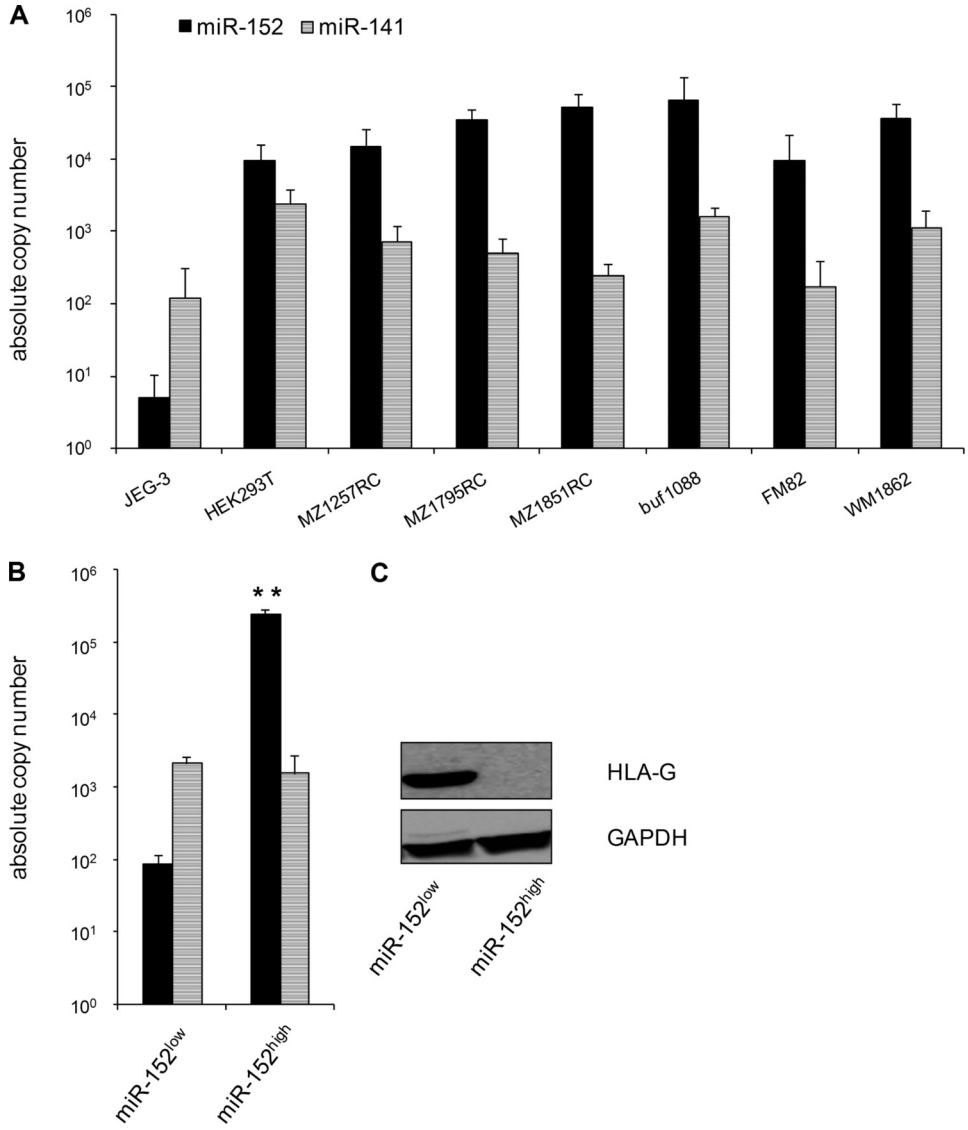

FIGURE 1. **Expression of miR-152, miR-141, and miR-541 in human tumor cell lines.** *A,* qPCR-based detection and quantification of the miR-152 deficiency in JEG-3 cells revealed a 1000-fold reduced expression of miR-152 compared with other human tumor cell lines analyzed (*HEK*, human embryonic kidney; *MZ*, renal cell carcinoma cells; melanoma cells). *B,* qPCR analysis of the miR-152 expression after reconstitution of miR-152 expression in JEG-3 cells. A comparison of the miR-152-expressing transfectants (miR-152^{high}) and the respective mock-control (miR-152^{low}) is shown. The expression of miR-141 (internal control) was not affected. *C,* miR-152-induced down-regulation of *HLA-G* in JEG-3 cells after reconstitution of miR-152 expression. As a consequence of the miR-152 reconstitution, the miR-152 target *HLA-G* was completely down-regulated in the miR-152-expressing transfectants (miR-152^{high}) compared with the mock-control (miR-152^{low}). A representative Western blot of three individual experiments with similar results is shown.

the secondary structure of the upstream 3′-UTR RNA sequence to guarantee the correct interactions with RNA-binding proteins and miRs.

Analysis of Clinical cDNA Microarrays for Detection of Correlations between 14-3-3β, HLA-G, and Patient Survival—Transcriptome data obtained from patient samples of various cancer types have been analyzed using the free on-line database R2, microarray analysis, and visualization platform to correlate the expression of *14-3-3β* (*YWHAB*) and *HLA-G* with the overall survival of tumor patients.

RESULTS

Reconstitution of miR-152 Expression in JEG-3 Cells, Establishment of the Model System—The expression pattern of the HLA-G-specific candidate miR-152 and miR-141, which served as an internal control, was determined in HLA-G$^+$ JEG-3 cells and different RCC and melanoma cell lines. The choriocarcinoma cell line JEG-3, but not the other cell lines tested, expressed low levels of miR-152 (Fig. 1*A*). This was in line with high levels of HLA-G protein in JEG3 cells, whereas the RCC and melanoma cells tested lack *HLA-G* expression (4, 16). Furthermore, miR-152 expression was restored in JEG-3 cells by stable transfection of an miR-152 expression plasmid resulting in ~1000-fold increase of the miR-152 copy number (Fig. 1*B*), which is physiologic and comparable with the transcripts found in HLA-G$^-$ tumor cells. This was accompanied by a loss of HLA-G protein expression (Fig. 1*C*). The miR-152-induced down-regulation of *HLA-G* expression proves the functionality of the overexpressed miR-152. In contrast, miR-141 expression used as internal control remained unaffected in miR-152^{high} cells (Fig. 1*B*).

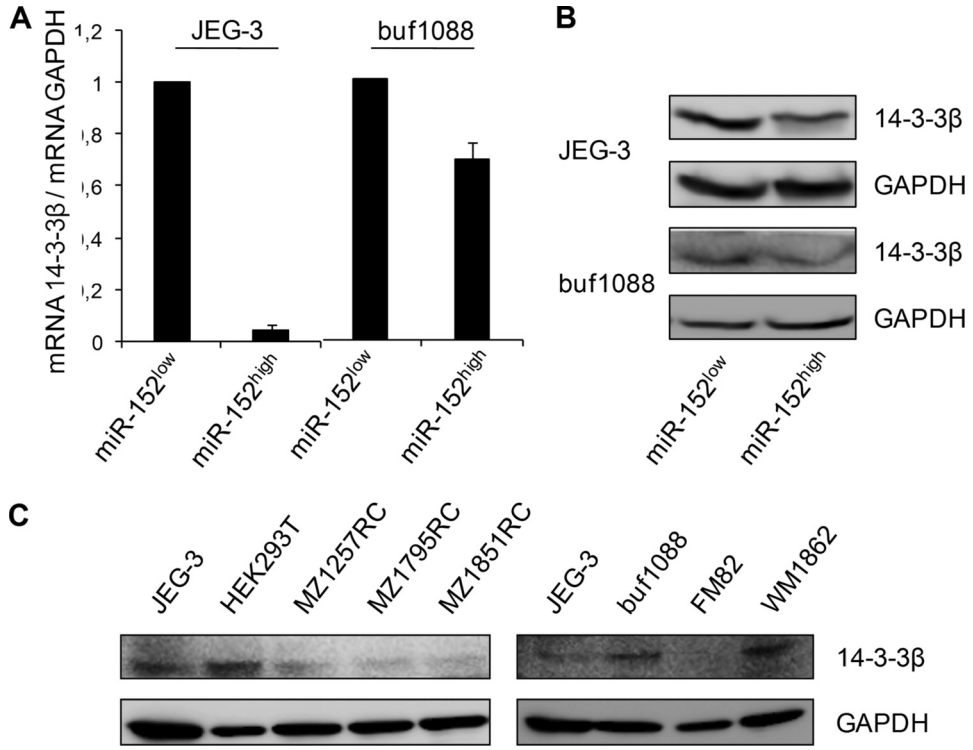

FIGURE 2. **Validation of 14-3-3β as a novel miR-152 target by qPCR and Western blot analysis.** *A,* relative *14-3-3β* mRNA expression in the stable miR-152^{high} transfectant of JEG-3 and Buf1088 cells demonstrates a strong down-regulation of the *14-3-3β* (*YWHAB*) transcription. *B,* protein expression of *14-3-3β* in the stable miR-152 transfectants of JEG-3 and Buf1088. Western blot analysis demonstrates a down-regulation of the 14-3-3β protein upon miR-152 overexpression. *C,* monitoring of 14-3-3β protein in different cell systems. A heterogeneous protein expression of the 14-3-3β protein in the different cell lines was found (*HEK,* human embryonic kidney; *MZ,* renal cell carcinoma cells; melanoma cells). A correlation between miR-152 and *14-3-3β* could not be observed in the applied cell lines indicating that also other mechanisms could contribute to the regulation of *14-3-3β*.

Identification of Novel miR-152 Targets by Proteome Analysis—To determine novel targets of miR-152, the protein expression pattern of mock-transfected (miR-152^{low}) and miR-152-transfected JEG-3 cells (miR-152^{high}) was compared using 2DE-based proteome analysis. Differentially expressed protein spots of miR-152^{low} *versus* miR-152^{high} model systems were then subjected to mass spectrometric analysis. As listed in Table 1, 24 proteins were differentially expressed upon miR-152 overexpression, from which 14 proteins were down-regulated and 10 proteins were up-regulated in miR-152^{low} *versus* miR-152^{high} JEG-3 cells. Regarding their classification, these proteins are mainly involved in metabolism and biogenesis (Table 1 and Fig. 7). Because 14-3-3 proteins are associated with oncogenic features (30) that could explain the observed differences in proliferation upon miR-152 overexpression (described below), further studies focused on the expression, function, and regulation of *14-3-3β* by miR-152.

Validation of 14-3-3β as a Specific miR-152 Target—The strong miR-152-mediated down-regulation of *14-3-3β* mRNA and protein expression was validated by qPCR (Fig. 2, *A* and *B*) and Western blot analysis of miR-152^{low} *versus* miR-152^{high} JEG-3 and Buf1088 cells. It is noteworthy that the 14-3-3β protein is heterogeneously expressed in the different (tumor) cells analyzed. Although it was not detectable or only barely detectable in the melanoma cell line FM82 or in the RCC cell lines, respectively, the highest expression levels of 14-3-3β protein were found in Buf1088 and WM1862 cells (Fig. 2*C*). Because only JEG-3 cells exert a miR-152 deficiency, a correlation between miR-152 and 14-3-3β protein in these cells could not be observed. In this context, it is noteworthy that 14-3-3β down-regulation might be also attributed to other mechanisms, such as epigenetic silencing, mutation, or dysregulation of p53 or its rapid degradation due to its ubiquination as reported for 14-3-3σ (31, 32).

Direct Interaction between miR-152 and the 14-3-3β 3′-UTR—*In silico* analyses of the miR-152 binding to the target mRNA of *14-3-3β* were performed demonstrating that miRanda, miRDB, miRwalk, TargetScan, and RNA hybrid predict a miR-152-binding site (33–36). To further study the interaction between miR-152 and *14-3-3β,* a fragment of the *14-3-3β* 3′-UTR, including the *in silico* predicted miR-152-binding site, was cloned behind the luc reporter gene. A deletion (Δ) construct lacking the *in silico* predicted miR-152-binding site served as control (Fig. 3*D*). These constructs were co-transfected with the miR expression vectors pmR(mock), pmR(miR-152), and pmR(miR-541) as nonsense control, which so far only affects neuronal differentiation (37). As shown in Fig. 3*A*, a significantly reduced luc activity was detected by co-transfection with the miR-152 expression vector. However, this inhibition was completely abolished by deleting the *in silico* predicted miR-152-binding site in the reporter gene construct.

To further investigate the effect of miR-152 on the 3′-UTR of *14-3-3β,* this miR was inhibited by a miR-152 decoy construct. By blocking miR-152, the luc activity in combination with the 3′-UTR of *14-3-3β* was significantly stabilized when compared with the respective mock controls (Fig. 3*B*).

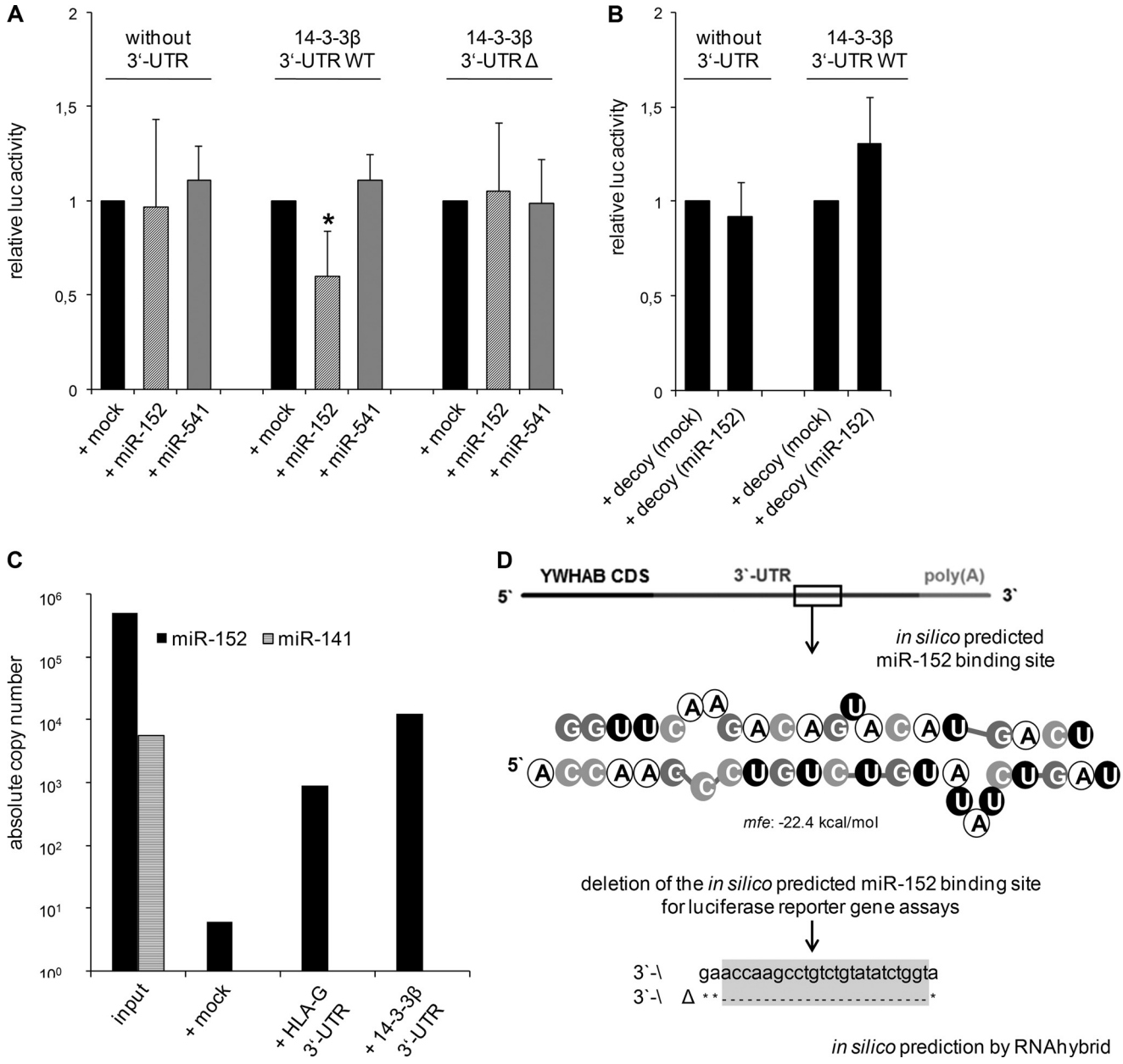

FIGURE 3. **Direct interaction between the 3′-UTR of *14-3-3β* and the miR-152.** *A,* luciferase reporter gene assay. The activity of the luc construct lacking any 3′-UTR was not affected by the expression of miR-152 and miR-541 (negative control miR). In contrast, cloning the *14-3-3β* 3′-UTR behind the luc reporter gene in combination with the miR-152 transfection leads to a significant reduction of the relative luc reporter gene activity. However, co-transfection of miR-541 as nonsense control and of the pmR-mock vector had no effect on the relative luc reporter gene activity. The deletion (Δ) of the *in silico* predicted miR-152-binding site completely restored the reductive effect of miR-152 on the 14-3-3*β* 3′-UTR (*, *t* test; $p < 0.05$). *B,* to block miR-152 activity, an miR-152-specific decoy was cloned according to Haraguchi *et al.* (25) and combined in the luc reporter gene assay, resulting in an increased luc activity of the *14-3-3β* 3′-UTR upon miR-152 blocking compared with respective mock controls. *C,* applying a novel miR enrichment assay (26), the direct interaction of miR-152 and the *14-3-3β* 3′-UTR can be demonstrated. The input shows the available amount of miR-152 and as internal control miR-141 in the used cell lysate. There was no enrichment of miR-152 in the absence of the 3′-UTR as bait (<10 copies = background). In contrast with the *HLA-G* 3′-UTR (positive control) and even more effective with the *14-3-3β* 3′-UTR as bait, miR-152 was strongly enriched out of the cell lysate. The internal negative control miR-141, present in the input, was not enriched. *D,* scheme of the *in silico* analysis for putative miR-152-binding site within the *14-3-3β* (*YWHAB*) 3′-UTR.

Furthermore, the wild type (WT) 3′-UTRs of *14-3-3β* and *HLA-G* were employed for miTRAP to enrich miRs from the *HLA-G* mRNA$^+$/HLA-G protein$^-$ RCC MZ2905RC cell line. The principle of the miTRAP experiment is shown in Fig. 8. Using the *HLA-G* 3′-UTR as bait (positive control), miR-152 could be enriched, whereas miR-141 (internal negative control) was not enriched due to the lack of a binding site in the 3′-UTR of *HLA-G* and of *14-3-3β*. Interestingly, the enrichment of miR-152 using the *14-3-3β* WT 3′-UTR was 10 times higher when compared with that of the *HLA-G* 3′-UTR (Fig. 3*C*).

Altered Growth Properties and Apoptosis Sensitivity of 14-3-3β Transfectants—Because *14-3-3β* could exert anti-apoptotic activity, promote tumor proliferation, and decrease overall survival of tumor patients (11, 38–41), the impact of an altered *14-3-3β* expression in the miR-152^{high} JEG-3 cells (miR-152-overexpressing transfectants) was determined. Therefore, the

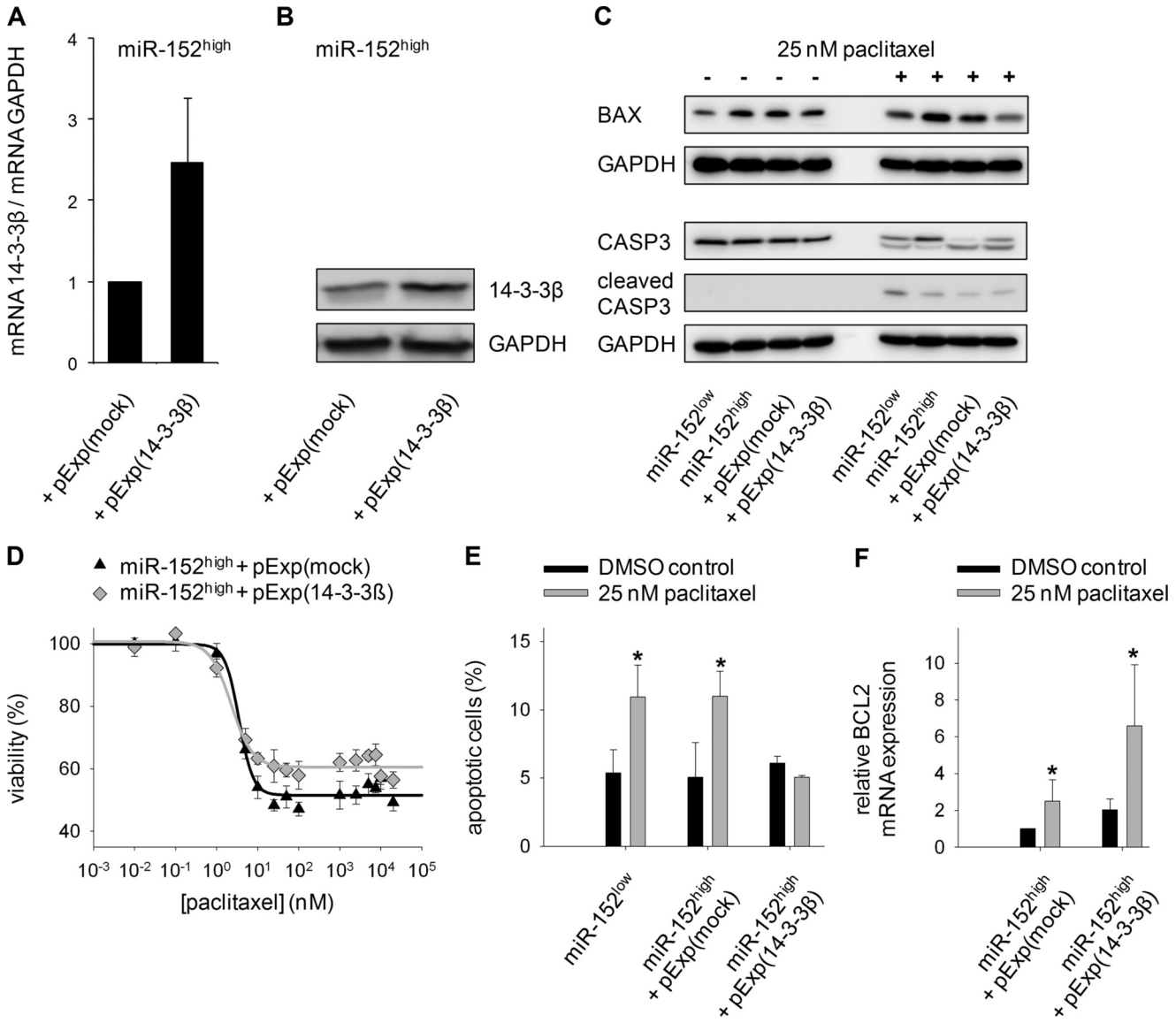

FIGURE 4. **Reconstitution of the *14-3-3β* expression and apoptosis assays.** *A* and *B*, analysis of the reconstitution of the *14-3-3β* expression in the miR-152 transfectants of JEG-3 by stable transfection with an expression vector (*pExp*) encoding the *14-3-3β* coding sequence without 3′-UTR by qPCR (*A*) and Western blot (*B*). *C*, miR-152-induced up-regulation of BAX protein. Before the detection of BAX protein, the transfectants were cultured for 72 h in the absence and presence of 25 nM paclitaxel. Increased levels of the proapoptotic protein BAX were detected in all miR-152^{high} transfectants in the absence of paclitaxel but with no concomitant effect on the cleaved caspase 3 levels. In the presence of paclitaxel, reconstitution of the anti-apoptotic 14-3-3β protein reduced the BAX protein level but had no effect on cleaved caspase 3. *D*, decreased sensitivity toward drug treatment with paclitaxel upon 14-3-3β reconstitution. Cells were grown for 72 h in the absence or presence of various concentrations of paclitaxel (0–20 μM) and analyzed via XTT assay using the XTT cell proliferation kit (Roche Applied Science) according to the manufacturer's protocol. *E*, detection of altered apoptosis sensitivity in the distinct JEG-3 transfectants using annexin V and 7-amino-actinomycin D staining. Before the detection of the apoptotis rates, the transfectants were cultured for 72 h in the absence and presence of 25 nM paclitaxel. Whereas the apoptosis sensitivity of untreated transfectants (DMSO control) remained unaffected, a reduction of the paclitaxel-induced apoptosis was detected after *14-3-3β* reconstitution. *, *t* test; $p < 0.05$. *F*, up-regulation of *BCL2* gene expression after *14-3-3β* reconstitution was detected after 72 h of incubation in the absence and presence of 25 nM paclitaxel. *, *t* test; $p < 0.05$.

down-regulated *14-3-3β* expression was reconstituted by stable overexpression of the *14-3-3β* coding sequence without the 3′-UTR into miR-152^{high} JEG-3 cells leading to an ~3-fold increase in *14-3-3β* transcript (Fig. 4*A*) and protein levels (Fig. 4*B*). The miR-152-mediated down-regulation of the *14-3-3β* expression upon miR-152 overexpression resulted in an up-regulation of the pro-apoptotic protein BAX, whereas the level of cleaved caspase 3 and the content of early apoptotic cells remained unaffected (Fig. 4, *C* and *E*) in untreated cells. In contrast, treatment with 25 nM paclitaxel for 72 h reduced the level of pro-apoptotic BAX within the *14-3-3β*-expressing rescue variant (Fig. 4*C*). Furthermore, treatment with 25 nM paclitaxel for 72 h increased the number of early apoptotic cells about 50% in both miR-152^{low} and miR-152^{high} cells, although overexpression of the anti-apoptotic *14-3-3β* rescue variant lacking the 3′-UTR significantly reduced apoptosis sensitivity (Fig. 4*E*).

The reconstitution of the 14-3-3β protein in the miR-152^{high} cells resulted in a significant down-regulation of apoptosis, which could be explained by the detected up-regulation of the transcription level of the anti-apoptotic *BCL2* gene (Fig. 4*F*). The presence of paclitaxel alone already induced the up-regu-

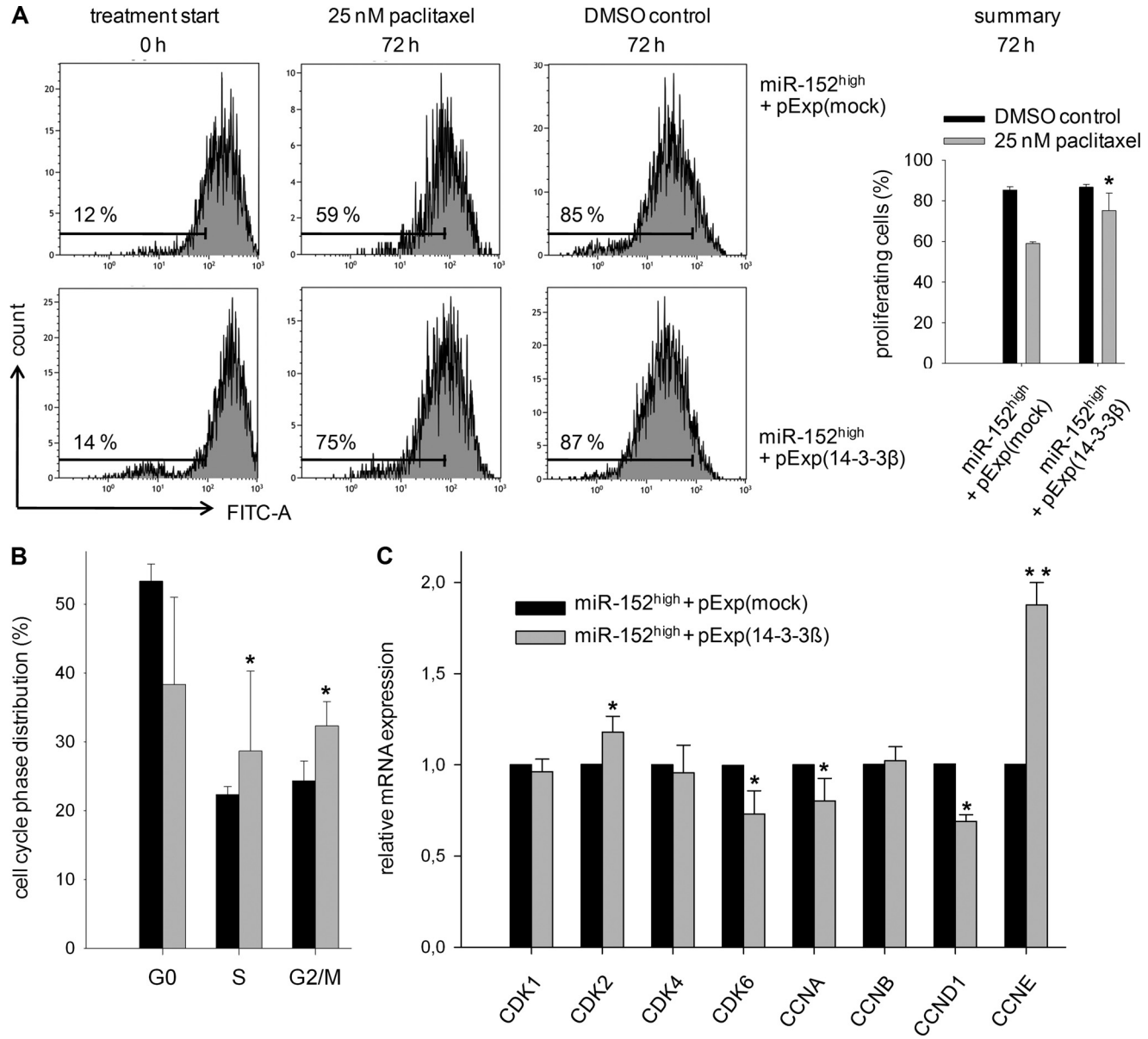

FIGURE 5. **Role of *14-3-3β* for cell proliferation.** *A,* flow cytometry analysis of CFSE-stained JEG-3 transfectants after 72 h of incubation in the absence or presence of 25 nM paclitaxel revealed a paclitaxel-induced reduction of the proliferation rate of the miR-152-expressing transfectants due to *14-3-3β* down-regulation and the reversal of this effect due to *14-3-3β* reconstitution, whereas the proliferation rate of untreated transfectants (DMSO control) remained unaffected. The number provided within the given profile highlights the percentage of proliferating cells. The *bar chart* at right summarizes the results based on three independent experiments. *t* test; $p < 0.05$. *B,* analyzing the cell cycle revealed that the reconstitution of the 14-3-3β protein in the miR-152 overexpressing transfectants enhances the percentage of mitotic cells (M-phase) *t* test; $p < 0.05$. *C,* quantitation of the gene expression of distinct cyclins and cyclin-dependent kinases involved in the cell cycle regulation showed a strong increase in the expression of *CCNE* and *CDK2* resulting in an enhanced transition from G_1 to S phase. *, *t* test; $p < 0.05$; **, *t* test; $p < 0.005$.

lation of *BCL2* gene expression, but this effect was strongly increased upon *14-3-3β* reconstitution.

To address the clinical relevance of the *14-3-3β*-mediated effects on the apoptosis, the transfectants with the highest difference in the *14-3-3β* expression (miR-152^{high} + pExp(mock) and miR-152^{high} + pExp(*14-3-3β*)) were treated with different concentrations (0–20 μM) of the chemotherapeutic drug paclitaxel.

The cytotoxic effects were monitored at different drug concentrations to define the respective 50% proliferation/growth inhibition concentration (IC_{50}) values via XTT assays. As shown in Fig. 4*D,* a dose-dependent but incomplete inhibition of cell viability was detected in the presence of paclitaxel.

However, upon drug treatment there were no significant changes within the IC_{50} values for paclitaxel (3.2 ± 0.5 nM), but the residual metabolic activity increased from 52 ± 3 to 62 ± 3% in the presence of paclitaxel when compared with the miR-152^{high}/14-3-3β^{low} cells (Fig. 4*D*). Furthermore, high expression levels of *14-3-3β* could be correlated to a poor overall survival of patients of distinct cancer diseases (Fig. 6).

In coincidence with the previously described function as a tumor suppressor, the miR-152-mediated down-regulation of *14-3-3β* decreased the proliferation rate in the presence of 25 nM paclitaxel at an average of about 11%, whereas the expression of the *14-3-3β* rescue variant enhanced the proliferative

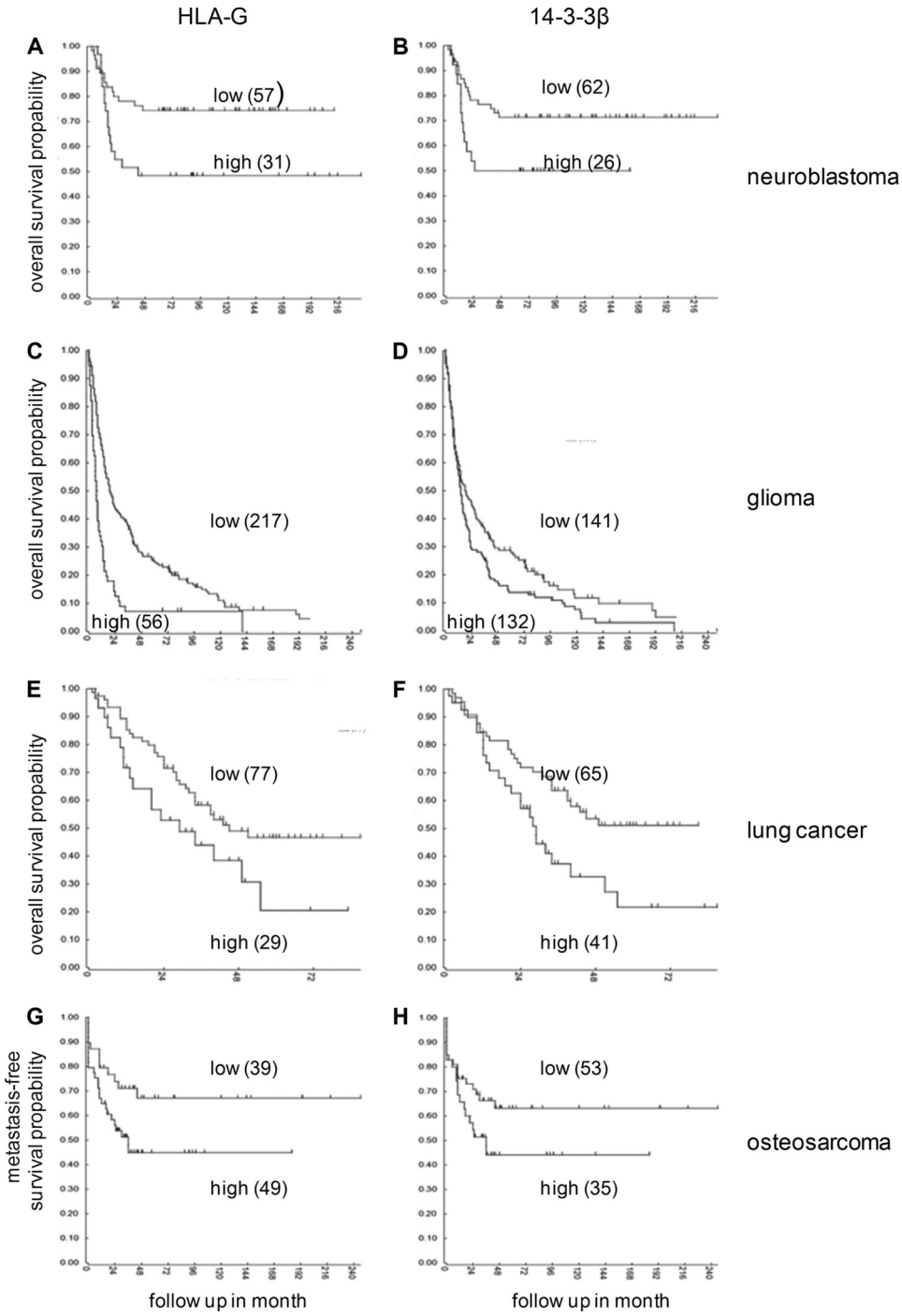

FIGURE 6. **Correlation of the expression of *HLA-G* and *14-3-3β* with overall patient survival in distinct tumor entities.** *A–H,* higher the expression of the miR-152 targets *HLA-G* and *14-3-3β,* the worse is the overall survival of the patients. *A* and *B,* neuroblastoma; *C* and *D,* glioma; *E* and *F,* lung cancer; *G* and *H,* osteosarcoma. The plots are based on transcriptional quantifications. The analysis was performed using the on-line database R2, microarray analysis and visualization platform.

capacity of these cells from 59 to 75% significantly as measured by flow cytometry after CFSE labeling and incubation for 72 h in the presence of 25 nM paclitaxel (Fig. 5*A*). In the absence of the chemotherapeutic drug, no differences on the cell proliferation capacity (85 to 87% proliferating cells) were detected. To further characterize the proliferation rate upon 14-3-3β protein overexpression, cell cycle analysis of the JEG-3 transfectants miR-152^{high} + pExp (mock) and miR-152^{high} + pExp(14-3-3β) was performed.

As shown in Fig. 5*B,* the *14-3-3β* reconstitution resulted in a significantly increased number of mitotic cells in miR-152-overexpressing JEG-3 cells (miR-152^{high} + pExp(*14-3-3β*). In addition, the expression of genes involved in cell cycle regulation was analyzed by qPCR.

Although cyclin B and the cyclin-dependent kinases 1 and 4 showed no differential expression at the transcript level, gene expression of cyclin E and cyclin-dependent kinase 2 were significantly up-regulated upon 14-3-3β protein expression,

therefore enhancing G_1 to S cell cycle phase transition, determining the cell division. In contrast, cyclin A and D and cyclin-dependent kinase 6 were down-regulated (Figs. 5*C* and 8*C*).

Correlation of 14-3-3β and HLA-G Expression with Patient Survival—The expression of both *HLA-G* and *14-3-3β* is controlled by miR-152. Whereas *HLA-G* allows tumors to escape the immune system, *14-3-3β* decreases the sensitivity of tumor cells to apoptosis (Fig. 6) (38–40, 42). To determine whether the expression of both genes could be correlated with clinical parameters, *in vivo* cDNA microarrays were analyzed using patients' data from various cancer entities (neuroblastoma, lung cancer, glioma, and osteosarcoma) obtained from the R2 on-line database. Unfortunately, no RCC or melanoma data sets were available in the database. However, the patients' cohorts characterized by high *HLA-G* or high *14-3-3β* mRNA expression levels revealed a significantly decreased overall survival of patients when compared with that characterized by low expression levels of both genes. As illustrated in Fig. 5, the expression and the survival data of these two miR-152 targets could be directly correlated, thereby strengthening the prognostic potential of *HLA-G*, *14-3-3β*, and miR-152 expression in various cancer types.

DISCUSSION

In this study, a novel miR-152 target, the protein 14-3-3β, was identified by comparative 2DE-based proteomic profiling of miR-152-overexpressing transfectants and control cells. Because the choriocarcinoma cell line JEG-3 expressed very low levels of miR-152, this miR was stably overexpressed in JEG-3 cells, which resulted in a down-regulation of the known miR-152 target *HLA-G* (4), thereby demonstrating the functionality of the model system.

Recently, 2DE-based proteomics has been employed as a strategy to identify novel miR targets (43). One advantage of proteome-based methods for miR target identification compared with transcriptome-based technologies is the readout at the protein level, because miRs must not induce mRNA decay but miR binding leads to translational repression of the target mRNAs (44).

The comparison of the protein expression patterns of mock- and miR-152-transfected JEG-3 cells (miR-152^{low} *versus* miR-152^{high}) led to the identification of 24 differentially expressed proteins, which are mainly involved in cellular metabolism and biogenesis (Table 1 and Fig. 7) As miR-152 was shown to be a tumor-suppressive miR, and its expression is associated with a decreased cell proliferation and an increased apoptosis (11–14), the following studies focused on the novel anti-apoptotic miR-152 target 14-3-3β, a phosphoserine/phosphothreonine-binding protein that was down-regulated upon miR-152 expression. The highly conserved 14-3-3 protein family plays a key role in various cellular processes, such as metabolism, protein trafficking, signal transduction, apoptosis, and cell cycle regulation. Because many interactions of 14-3-3 members with other proteins are phosphorylation-dependent, 14-3-3β has been tightly integrated into the core phospho-regulatory pathways that are crucial for normal growth and development and often become deregulated in human malignancies, including cancer (45). *14-3-3β* exerts anti-apoptotic activity, promotes tumor proliferation, and decreases overall survival of hepatocellular carcinoma patients (11). In the context of the post-transcriptional regulation of *14-3-3β* by the tumor-suppressive miR-152,

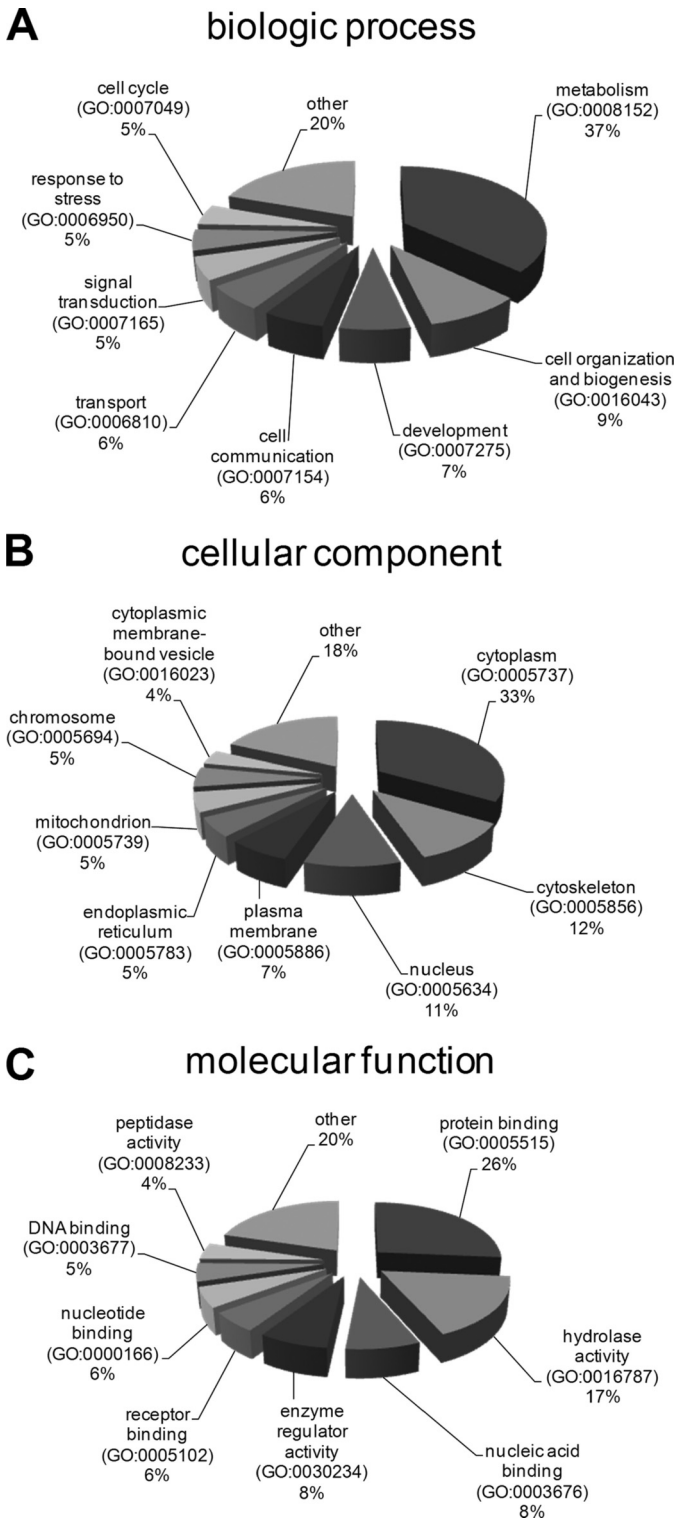

FIGURE 7. **Annotation clustering of the differentially expressed proteins upon miR-152 overexpression in JEG-3 cells identified by 2DE-based proteomic profiling and mass spectrometry.** The differentially expressed proteins upon miR-152 overexpression in JEG-3 cells identified by 2DE-based proteomic profiling and mass spectrometry were grouped according to their GO annotations for their biologic process (*A*), cellular localization (*B*), and to their molecular functions (*C*).

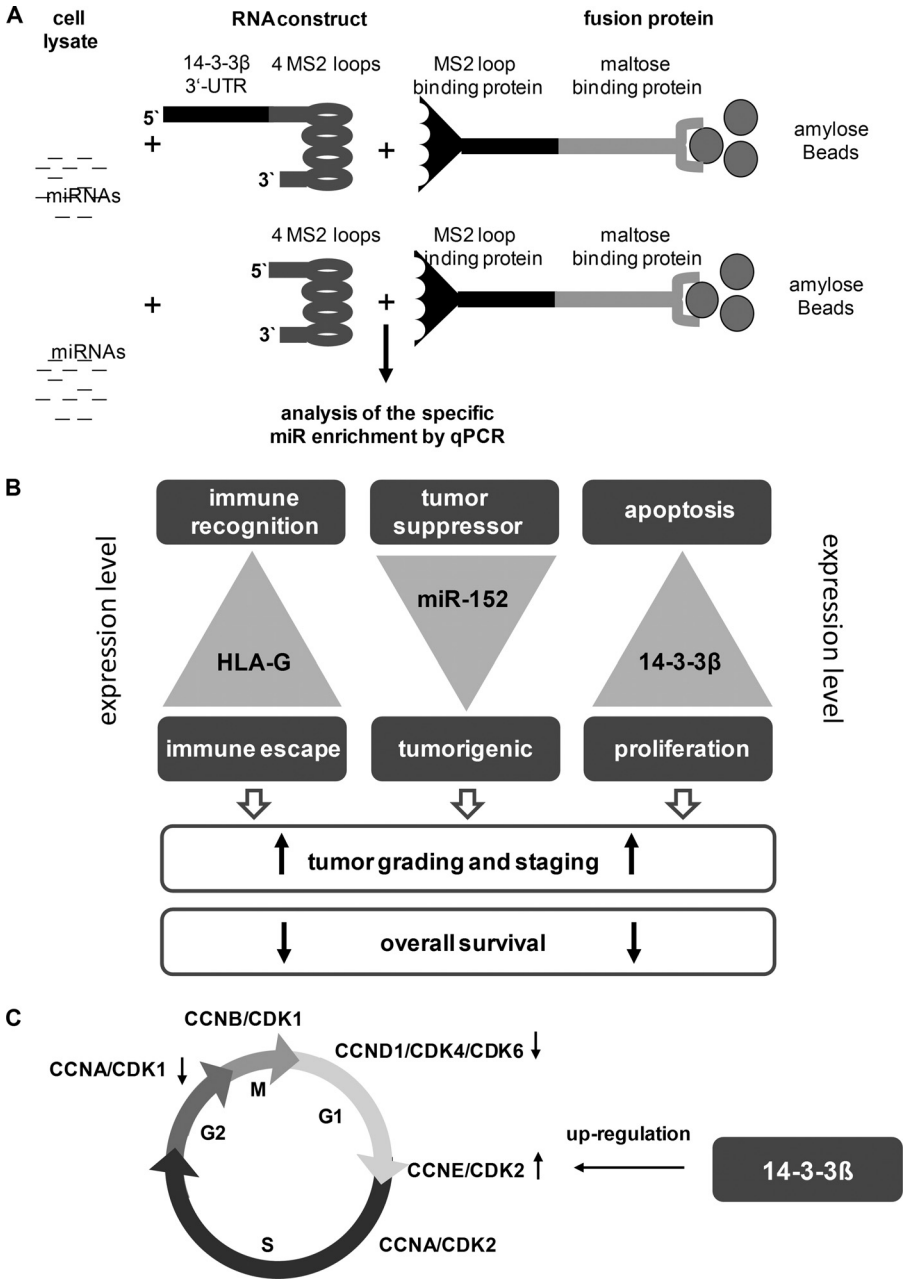

FIGURE 8. **Principle of the miR enrichment assay miTRAP (*A*), hypothesis of the dual role of miR-152 as tumor suppressor (*B*), and influence of *14-3-3β* on the cell cycle (*C*).** *A,* scheme of the miR enrichment assay miTRAP. An *in vitro* transcribed synthetic RNA construct, consisting of the 3′-UTR of interest and four MS2 loops, is employed as bait for specific miR enrichment out of a cell lysate (MZ2905RC; *HLA-G* mRNA+/protein−). These RNA constructs are loaded on amylose beads for a specific enrichment of miRs by applying a fusion protein of MS2 loop-binding protein and maltose-binding protein (26). *B,* working hypothesis demonstrating that a defect in the expression of the miR-148 family affects the expression of *HLA-G* and *14-3-3β* altering the immunogenicity and the tumorigenicity for tumor cells. *C,* scheme of the cell cycle and involved cyclins and cyclin-dependent kinases; altered after Bonelli *et al.* (52).

14-3-3β exerts anti-apoptotic activities thereby enhancing the viability of the respective transfectants upon treatment with the chemotherapeutic drug paclitaxel due to a significant up-regulation of *BCL2*. This is in line with an increased proliferation of tumor cells by up-regulation of the CCNE-CDK2 complex. The analysis of patients surviving certain tumor entities demonstrates a direct inverse correlation of the *14-3-3β* expression levels with the overall survival rate of tumor patients. Furthermore, these data are in line with a high frequency of *14-3-3β* overexpression in human tumors of distinct origin, which is also often accompanied by a reduced apoptosis sensitivity.

The direct interaction of *14-3-3β* and miR-152 was characterized using luc reporter gene analyses and with the miR-152 blocking experiment and miR enrichment assay (miTRAP). Using a region of the 3′-UTR of *14-3-3β* (2414–3067 bp of the mRNA sequence) containing the *in silico* predicted miR-152-binding site as bait for the specific miRNA enrichment assay (miTRAP) revealed a specific enrichment of miR-152 from MZ2905RC cell lysate (Fig. 3*B*). Functional studies further demonstrated an anti-apoptotic activity of 14-3-3*β*, which might also have clinical relevance and might serve as a prognostic factor for tumor patients.

The 14-3-3 proteins dimerize to homo- and heterodimers, which interact with a large number of cellular proteins, including transcription factors, cytoskeletal proteins, signaling molecules, apoptosis factors, and tumor suppressors (38, 46, 47). Factors involved in apoptosis, which were inhibited by 14-3-3 proteins, are the pro-apoptotic proteins BAX- and BCL2-associated agonist of cell death (BAD) (39, 40). These data are in line with the miR-152-mediated down-regulation of 14-3-3β, which resulted in increased BAX protein levels (Fig. 4*C*) as well as in decreased *BCL2* gene expression (Fig. 4*F*). Furthermore, the decreased sensitivity toward the chemotherapeutic drug paclitaxel after reconstitution of *14-3-3β* expression indicated a clinical relevance of the novel miR-152 target 14-3-3β.

In addition, analysis of cDNA microarrays with known clinical parameters, including patients' survival data, revealed that *14-3-3β* and *HLA-G* share a common regulation mechanism, and their high expression levels could be correlated with a poor overall survival of patients with tumors. The miR-152-mediated regulation of both *14-3-3β* and *HLA-G* links the *HLA-G*-induced immune escape mechanism with *14-3-3β*-associated transformed growth properties of tumors (Fig. 8*B*).

In accordance with these data, *14-3-3β* and *-ζ* have been demonstrated to be often overexpressed in human tumors of distinct origin and have been suggested as clinically relevant prognostic biomarkers due to their association with tumor progression and poor patient survival (11, 48, 49). This might allow the identification of tumor patients with poor prognosis to receive a more aggressive treatment. Even more interesting, the expression levels of *14-3-3β* were higher in urine samples from patients with RCC than in samples from healthy volunteers, and therefore *14-3-3β* may be a diagnostically useful biomarker for early diagnosis of this disease (50).

In conclusion, this study not only extended previously identified possible direct targets of miR-152, like *HLA-G, DNMT-1, E2F3, MET,* and *RICTOR*, to *14-3-3β* suggesting that its silencing contributes to tumorigenesis, but identified for the first time a dual role of miR-152 by modulating not only the growth characteristics of tumor cells but also immune surveillance (4, 12, 51). Thus, miR-148 family members might serve as potential diagnostic and prognostic markers and provide novel treatment strategy for tumors, which is in line with its postulated tumor suppressor activity described in recent studies (12–14). However, further *in vivo* studies are required to confirm that miR-152 acts as a tumor suppressor by inhibiting both tumor growth and enhancing immunogenicity.

Acknowledgments—We thank Sylvi Magdeburg and Nicole Ott for excellent secretarial help and Dr. Jessica Bell for information about the R2 database.

REFERENCES

1. Berezikov, E. (2011) Evolution of microRNA diversity and regulation in animals. *Nat. Rev. Genet.* **12,** 846–860
2. Kozomara, A., and Griffiths-Jones, S. (2011) miRBase: integrating microRNA annotation and deep-sequencing data. *Nucleic Acids Res.* **39,** D152–D157
3. Grimson, A., Farh, K. K., Johnston, W. K., Garrett-Engele, P., Lim, L. P., and Bartel, D. P. (2007) MicroRNA targeting specificity in mammals: determinants beyond seed pairing. *Mol. Cell* **27,** 91–105
4. Manaster, I., Goldman-Wohl, D., Greenfield, C., Nachmani, D., Tsukerman, P., Hamani, Y., Yagel, S., and Mandelboim, O. (2012) miRNA-mediated control of HLA-G expression and function. *PLoS ONE* **7,** e33395
5. Amiot, L., Ferrone, S., Grosse-Wilde, H., and Seliger, B. (2011) Biology of HLA-G in cancer: a candidate molecule for therapeutic intervention? *Cell. Mol. Life Sci.* **68,** 417–431
6. Bukur, J., Jasinski, S., and Seliger, B. (2012) The role of classical and non-classical HLA class I antigens in human tumors. *Semin. Cancer Biol.* **22,** 350–358
7. Dunker, K., Schlaf, G., Bukur, J., Altermann, W. W., Handke, D., and Seliger, B. (2008) Expression and regulation of non-classical HLA-G in renal cell carcinoma. *Tissue Antigens* **72,** 137–148
8. Kulkarni, S., Savan, R., Qi, Y., Gao, X., Yuki, Y., Bass, S. E., Martin, M. P., Hunt, P., Deeks, S. G., Telenti, A., Pereyra, F., Goldstein, D., Wolinsky, S., Walker, B., Young, H. A., and Carrington, M. (2011) Differential microRNA regulation of HLA-C expression and its association with HIV control. *Nature* **472,** 495–498
9. Almeida, C. R., Ashkenazi, A., Shahaf, G., Kaplan, D., Davis, D. M., and Mehr, R. (2011) Human NK cells differ more in their KIR2DL1-dependent thresholds for HLA-Cw6-mediated inhibition than in their maximal killing capacity. *PLoS ONE* **6,** e24927
10. Almeida, C. R., and Davis, D. M. (2006) Segregation of HLA-C from ICAM-1 at NK cell immune synapses is controlled by its cell surface density. *J. Immunol.* **177,** 6904–6910
11. Liu, T. A., Jan, Y. J., Ko, B. S., Chen, S. C., Liang, S. M., Hung, Y. L., Hsu, C., Shen, T. L., Lee, Y. M., Chen, P. F., Wang, J., Shyue, S. K., and Liou, J. Y. (2011) Increased expression of 14-3-3β promotes tumor progression and predicts extrahepatic metastasis and worse survival in hepatocellular carcinoma. *Am. J. Pathol.* **179,** 2698–2708
12. Tsuruta, T., Kozaki, K., Uesugi, A., Furuta, M., Hirasawa, A., Imoto, I., Susumu, N., Aoki, D., and Inazawa, J. (2011) miR-152 is a tumor suppressor microRNA that is silenced by DNA hypermethylation in endometrial cancer. *Cancer Res.* **71,** 6450–6462
13. Xiang, Y., Ma, N., Wang, D., Zhang, Y., Zhou, J., Wu, G., Zhao, R., Huang, H., Wang, X., Qiao, Y., Li, F., Han, D., Wang, L., Zhang, G., and Gao, X. (2014) miR-152 and miR-185 co-contribute to ovarian cancer cells cisplatin sensitivity by targeting DNMT1 directly: a novel epigenetic therapy independent of decitabine. *Oncogene* **33,** 378–386
14. Zhu, C., Li, J., Ding, Q., Cheng, G., Zhou, H., Tao, L., Cai, H., Li, P., Cao, Q., Ju, X., Meng, X., Qin, C., Hua, L., Shao, P., and Yin, C. (2013) miR-152 controls migration and invasive potential by targeting TGFα in prostate cancer cell lines. *Prostate* **73,** 1082–1089
15. Sanfiorenzo, C., Ilie, M. I., Belaid, A., Barlési, F., Mouroux, J., Marquette, C. H., Brest, P., and Hofman, P. (2013) Two panels of plasma microRNAs as non-invasive biomarkers for prediction of recurrence in resectable NSCLC. *PLoS ONE* **8,** e54596
16. Zhu, X. M., Han, T., Wang, X. H., Li, Y. H., Yang, H. G., Luo, Y. N., Yin, G. W., and Yao, Y. Q. (2010) Overexpression of miR-152 leads to reduced expression of human leukocyte antigen-G and increased natural killer cell mediated cytolysis in JEG-3 cells. *Am. J. Obstet. Gynecol.* **202,** 592.e591–597
17. Bukur, J., Rebmann, V., Grosse-Wilde, H., Luboldt, H., Ruebben, H., Drexler, I., Sutter, G., Huber, C., and Seliger, B. (2003) Functional role of human leukocyte antigen-G up-regulation in renal cell carcinoma. *Cancer Res.* **63,** 4107–4111
18. Herrmann, F., Trowsdale, J., Huber, C., and Seliger, B. (2003) Cloning and functional analyses of the mouse tapasin promoter. *Immunogenetics* **55,** 379–388
19. Lichtenfels, R., Ackermann, A., Kellner, R., and Seliger, B. (2001) Mapping and expression pattern analysis of key components of the major histocompatibility complex class I antigen processing and presentation pathway in a representative human renal cell carcinoma cell line. *Electrophoresis* **22,** 1801–1809
20. Seliger, B., Fedorushchenko, A., Brenner, W., Ackermann, A., Atkins, D., Hanash, S., and Lichtenfels, R. (2007) Ubiquitin COOH-terminal hydrolase 1: a biomarker of renal cell carcinoma associated with enhanced tumor cell proliferation and migration. *Clin. Cancer Res.* **13,** 27–37
21. Chen, C., Ridzon, D. A., Broomer, A. J., Zhou, Z., Lee, D. H., Nguyen, J. T.,

Barbisin, M., Xu, N. L., Mahuvakar, V. R., Andersen, M. R., Lao, K. Q., Livak, K. J., and Guegler, K. J. (2005) Real-time quantification of microRNAs by stem-loop RT-PCR. *Nucleic Acids Res.* **33,** e179
22. Varkonyi-Gasic, E., Wu, R., Wood, M., Walton, E. F., and Hellens, R. P. (2007) Protocol: a highly sensitive RT-PCR method for detection and quantification of microRNAs. *Plant Methods* **3,** 12
23. Bukur, J., Herrmann, F., Handke, D., Recktenwald, C., and Seliger, B. (2010) Identification of E2F1 as an important transcription factor for the regulation of tapasin expression. *J. Biol. Chem.* **285,** 30419–30426
24. Stehle, F., Schulz, K., Fahldieck, C., Kalich, J., Lichtenfels, R., Riemann, D., and Seliger, B. (2013) Reduced immunosuppressive properties of axitinib in comparison with other tyrosine kinase inhibitors. *J. Biol. Chem.* **288,** 16334–16347
25. Haraguchi, T., Ozaki, Y., and Iba, H. (2009) Vectors expressing efficient RNA decoys achieve the long-term suppression of specific microRNA activity in mammalian cells. *Nucleic Acids Res.* **37,** e43
26. Braun, J., Misiak, D., Busch, B., Krohn, K., and Hüttelmaier, S. (2014) Rapid identification of regulatory microRNAs by miTRAP (miRNA trapping by RNA *in vitro* affinity purification). *Nucleic Acids Res.* **42,** e66
27. Köhn, M., Lederer, M., Wächter, K., and Hüttelmaier, S. (2010) Near-infrared (NIR) dye-labeled RNAs identify binding of ZBP1 to the noncoding Y3-RNA. *RNA* **16,** 1420–1428
28. Candiano, G., Bruschi, M., Musante, L., Santucci, L., Ghiggeri, G. M., Carnemolla, B., Orecchia, P., Zardi, L., and Righetti, P. G. (2004) Blue silver: a very sensitive colloidal Coomassie G-250 staining for proteome analysis. *Electrophoresis* **25,** 1327–1333
29. Zeeberg, B. R., Feng, W., Wang, G., Wang, M. D., Fojo, A. T., Sunshine, M., Narasimhan, S., Kane, D. W., Reinhold, W. C., Lababidi, S., Bussey, K. J., Riss, J., Barrett, J. C., and Weinstein, J. N. (2003) GoMiner: a resource for biological interpretation of genomic and proteomic data. *Genome Biol.* **4,** R28
30. Takihara, Y., Matsuda, Y., and Hara, J. (2000) Role of the β isoform of 14-3-3 proteins in cellular proliferation and oncogenic transformation. *Carcinogenesis* **21,** 2073–2077
31. Hermeking, H., Lengauer, C., Polyak, K., He, T. C., Zhang, L., Thiagalingam, S., Kinzler, K. W., and Vogelstein, B. (1997) 14-3-3 sigma is a p53-regulated inhibitor of G_2/M progression. *Mol. Cell* **1,** 3–11
32. Urano, T., Saito, T., Tsukui, T., Fujita, M., Hosoi, T., Muramatsu, M., Ouchi, Y., and Inoue, S. (2002) Efp targets 14-3-3 sigma for proteolysis and promotes breast tumour growth. *Nature* **417,** 871–875
33. Dweep, H., Sticht, C., Pandey, P., and Gretz, N. (2011) miRWalk–database: prediction of possible miRNA binding sites by "walking" the genes of three genomes. *J. Biomed. Inform.* **44,** 839–847
34. Krüger, J., and Rehmsmeier, M. (2006) RNAhybrid: microRNA target prediction easy, fast and flexible. *Nucleic Acids Res.* **34,** W451–W454
35. Lewis, B. P., Burge, C. B., and Bartel, D. P. (2005) Conserved seed pairing, often flanked by adenosines, indicates that thousands of human genes are microRNA targets. *Cell* **120,** 15–20
36. Wang, X. (2008) miRDB: a microRNA target prediction and functional annotation database with a wiki interface. *RNA* **14,** 1012–1017
37. Song, Y. X., Yue, Z. Y., Wang, Z. N., Xu, Y. Y., Luo, Y., Xu, H. M., Zhang, X., Jiang, L., Xing, C. Z., and Zhang, Y. (2011) MicroRNA-148b is frequently down-regulated in gastric cancer and acts as a tumor suppressor by inhibiting cell proliferation. *Mol. Cancer* **10,** 1
38. Gardino, A. K., and Yaffe, M. B. (2011) 14-3-3 proteins as signaling integration points for cell cycle control and apoptosis. *Semin. Cell Dev. Biol.* **22,** 688–695
39. Hermeking, H. (2003) The 14-3-3 cancer connection. *Nat. Rev. Cancer* **3,** 931–943
40. Nomura, M., Shimizu, S., Sugiyama, T., Narita, M., Ito, T., Matsuda, H., and Tsujimoto, Y. (2003) 14-3-3 Interacts directly with and negatively regulates pro-apoptotic Bax. *J. Biol. Chem.* **278,** 2058–2065
41. Zhao, J., Meyerkord, C. L., Du, Y., Khuri, F. R., and Fu, H. (2011) 14-3-3 proteins as potential therapeutic targets. *Semin. Cell Dev. Biol.* **22,** 705–712
42. Cai, M. Y., Xu, Y. F., Qiu, S. J., Ju, M. J., Gao, Q., Li, Y. W., Zhang, B. H., Zhou, J., and Fan, J. (2009) Human leukocyte antigen-G protein expression is an unfavorable prognostic predictor of hepatocellular carcinoma following curative resection. *Clin. Cancer Res.* **15,** 4686–4693
43. Diao, S., Zhang, J. F., Wang, H., He, M. L., Lin, M. C., Chen, Y., and Kung, H. F. (2010) Proteomic identification of microRNA-122a target proteins in hepatocellular carcinoma. *Proteomics* **10,** 3723–3731
44. Liu, J., Valencia-Sanchez, M. A., Hannon, G. J., and Parker, R. (2005) MicroRNA-dependent localization of targeted mRNAs to mammalian P-bodies. *Nat. Cell Biol.* **7,** 719–723
45. Morrison, D. K. (2009) The 14-3-3 proteins: integrators of diverse signaling cues that impact cell fate and cancer development. *Trends Cell Biol.* **19,** 16–23
46. Freeman, A. K., and Morrison, D. K. (2011) 14-3-3 Proteins: diverse functions in cell proliferation and cancer progression. *Semin. Cell Dev. Biol.* **22,** 681–687
47. Obsil, T., and Obsilova, V. (2011) Structural basis of 14-3-3 protein functions. *Semin. Cell Dev. Biol.* **22,** 663–672
48. Neal, C. L., and Yu, D. (2010) 14-3-3ζ as a prognostic marker and therapeutic target for cancer. *Expert Opin. Ther. Targets* **14,** 1343–1354
49. Nishimura, Y., Komatsu, S., Ichikawa, D., Nagata, H., Hirajima, S., Takeshita, H., Kawaguchi, T., Arita, T., Konishi, H., Kashimoto, K., Shiozaki, A., Fujiwara, H., Okamoto, K., Tsuda, H., and Otsuji, E. (2013) Overexpression of YWHAZ relates to tumor cell proliferation and malignant outcome of gastric carcinoma. *Br. J. Cancer* **108,** 1324–1331
50. Minamida, S., Iwamura, M., Kodera, Y., Kawashima, Y., Tabata, K., Matsumoto, K., Fujita, T., Satoh, T., Maeda, T., and Baba, S. (2011) 14-3-3 protein β/α as a urinary biomarker for renal cell carcinoma: proteomic analysis of cyst fluid. *Anal. Bioanal. Chem.* **401,** 245–252
51. Braconi, C., Huang, N., and Patel, T. (2010) MicroRNA-dependent regulation of DNA methyltransferase-1 and tumor suppressor gene expression by interleukin-6 in human malignant cholangiocytes. *Hepatology* **51,** 881–890
52. Bonelli, P., Tuccillo, F. M., Borrelli, A., Schiattarella, A., and Buonaguro, F. M. (2014) CDK/CCN and CDKI alterations for cancer prognosis and therapeutic predictivity. *Biomed. Res. Int.* **2014,** 361020
53. Pavan, L., Tarrade, A., Hermouet, A., Delouis, C., Titeux, M., Vidaud, M., Thérond, P., Evain-Brion, D., and Fournier, T. (2003) Human invasive trophoblasts transformed with simian virus 40 provide a new tool to study the role of PPARγ in cell invasion process. *Carcinogenesis* **24,** 1325–1336